Radiation Dose Distribution in Human Kidneys by Octreotides in Peptide Receptor Radionuclide Therapy

Mark Konijnenberg[1], Marleen Melis[2], Roelf Valkema[2], Eric Krenning[2], and Marion de Jong[2]

[1]Research and Development, Mallinckrodt Medical BV, Tyco Healthcare, Petten, The Netherlands; and [2]Department of Nuclear Medicine, Erasmus Medical Center, Rotterdam, The Netherlands

Ex vivo autoradiographs of healthy kidney tissue from patients who received ^{111}In-DTPA-octreotide (DTPA is diethylenetriaminepentaacetic acid) before nephrectomy showed very heterogeneous radioactivity patterns in the kidneys. The consequences of the reported inhomogeneities have been evaluated for radionuclide therapy with ^{90}Y- DOTA-Tyr^3-octreotide (DOTA is 1,4,7,10-tetraazacyclododecane-*N,N′,N″,N‴*-tetraacetic acid), ^{177}Lu-DOTA-Tyr^3-octreotate, and ^{111}In-DTPA-octreotide by calculating dose distributions and dose–volume histograms (DVHs) for the kidneys. **Methods:** Monte Carlo radiation transport calculations were performed by using the MCNP code version 5. The autoradiography data were used in a 2-dimensional model of the kidney tissue sections. A voxel structure inside the MIRD Pamphlet 19 multiregion kidney model was developed to generate a 3-dimensional representation of the autoradiographs. Dose distributions were calculated for the β-emitter ^{90}Y, the low-energy electron and γ-emitter ^{111}In, and the β- and γ-emitter ^{177}Lu. Isodose curves were generated for the 2-dimensional kidney sections and DVHs for the 3-dimensional kidney model. **Results:** The isodose curves for the high-energy β-emitter ^{90}Y did not show a sign of the inhomogeneous activity distribution, apart from the cortex–medulla boundaries. Both ^{111}In and ^{177}Lu isodose curves follow the autoradiographic activity distribution exactly. The 2 γ-rays from ^{111}In give higher doses to the low-radioactivity regions in the kidney sections. The DVHs show that the inhomogeneous activity distribution creates considerable volumes within the kidney and within the cortex with lower doses than the average kidney dose, together with volumes receiving much higher doses. This effect is most profound for ^{177}Lu, but also ^{111}In shows this heterogeneity in the dose distribution. **Conclusion:** Kidney dosimetry for radionuclide therapy can be based on average MIRD-based dose models for high-energy β-emitters (such as ^{90}Y). In contrast, low-energy β-emitters (such as ^{177}Lu) and Auger-electron–emitting radionuclides (such as ^{111}In) produce dose distributions in the kidneys that are very dependent on the activity distribution pattern in the kidney or renal cortex. Complication probability models for renal tissue damage after radionuclide therapy with these latter nuclides need to be developed, as the existing models based on average dose to the kidney or cortex from external beam therapy experience are most probably not valid.

Key Words: kidney dosimetry; dose volume histogram; ^{90}Y-DOTA-octreotide; ^{111}In-DTPA-octreotide; ^{177}Lu-DOTA-octreotate; radionuclide therapy

J Nucl Med 2007; 48:134–142

Radiolabeled somatostatin analogs such as ^{111}In-DTPA-octreotide (DTPA is diethylenetriaminepentaacetic acid) (OctreoScan; Mallinckrodt Medical BV) are most successful in detecting and imaging tumors expressing somatostatin receptors. As the receptor density is very high in certain types of tumors, often from neuroendocrine origin, therapeutic versions of the imaging compound were developed. Initially, trials with high activities of ^{111}In-DTPA-octreotide were performed; in later studies ^{90}Y-DOTA-Tyr^3-octreotide (DOTA is 1,4,7,10-tetraazacyclododecane-*N,N′,N″,N‴*-tetraacetic acid) (^{90}Y-edotreotide or ^{90}Y-DOTATOC) was used. At present ^{177}Lu-DOTA-Tyr^3-octreotate is under investigation for therapy of neuroendocrine tumors. For all radionuclide peptide combinations it is of crucial importance to design the optimal therapeutic window with the tumor dose as high as possible and the normal tissue dose as low as achievable. Radiation dosimetry for the normal organs at risk—that is, kidneys and bone marrow in radionuclide therapy—is essential for optimizing patient-tailored therapy.

The emphasis of dosimetry for peptide receptor radionuclide therapy (PRRT) is aimed at the dose-limiting organs: the kidneys. In the phase I trials of ^{90}Y-DOTA-Tyr^3-octreotide the dose to the kidneys was calculated according to the MIRD method (*1*). According to this method, it was assumed that the retained radioactivity of radiolabeled octreotide was homogeneously distributed over both kidneys. The only anatomic "patient specificity" was introduced by using either the male or female phantom with a slight difference in kidney mass (299 g for the male and 275 g for the female). All patients were scheduled for a maximum renal dose of 27 Gy. This limit was set higher than the gold standard for conventionally fractionated external beam therapy of 23 Gy, which results in a 5% probability of developing severe late kidney damage within 5 y (*2*). The dose rate at which the

Received Jun. 13, 2006; revision accepted Oct. 19, 2006.
For correspondence or reprints contact: Mark Konijnenberg, PhD, Mallinckrodt Medical BV, Postbus 3, 1755ZG Petten, The Netherlands.
E-mail: Mark.Konijnenberg@emea.tycohealthcare.com

kidney dose is given in PRRT is substantially lower than in external beam therapy, thus creating a situation with optimal possibilities for sublethal radiation damage repair, comparable to hyperfractionation.

The only reliable and to-this-date predictive dosimetry around the threshold for end-stage renal radiation disease has been performed for ^{90}Y-DOTA-Tyr^3-octreotide therapy. Before the first cycle of therapy the pharmacokinetics of renal uptake was determined for each patient by quantitative PET at 3 time points with the positron-emitting analog: ^{86}Y-DOTA-Tyr^3-octreotide (*3*). The cumulated activity in the kidneys for ^{90}Y was calculated and used to determine the maximum allowed activity for each patient. Indeed, less renal toxicity was observed in patients from this trial in comparison with other trials with a similar compound (DOTATOC), where individual patient dosing was based on radioactivity per unit body surface area (*4,5*). The encountered cases of nephrotoxicity could not be explained by the MIRD-based kidney dosimetry, as all patients received an average dose of 28 ± 3 Gy.

Retrospectively, a relation between the renal dose and renal toxicity could be proven when the dose was corrected for the actual kidney mass, the activity uptake in the cortex, and the relative biological effectiveness of the dose delivery, due to dose rate and fractionation of the therapy (*1,6,7*). Kidney dimensions were determined from the patient's abdominal CT images and were used to correct the renal cortex dosimetry based on MIRD Pamphlet 19 (MIRD19) (*8*). The number of therapy cycles and initial dose rates were of relevance for calculating biologic equivalent doses according to the linear-quadratic (LQ) model (*9*). Although many more patients have now been treated with ^{177}Lu-DOTA-Tyr^3-octreotate (*10*) and in the past with high-activity ^{111}In-DTPA-octreotide (*11*), no thorough patient-specific dosimetry evaluations are available.

PET using ^{86}Y-DOTA-Tyr^3-octreotide as well as SPECT using both ^{111}In-DTPA-octreotide and ^{177}Lu-DOTA-Tyr^3-octreotate indicates that most of the renal radioactivity was concentrated in the cortex of the kidneys (*12*). Ex vivo autoradiography of healthy renal tissue from renal cancer patients showed inhomogeneous distributions of ^{111}In-DTPA-octreotide in the cortex at millimeter-scale resolution (*13*). The ex vivo autoradiographs of the kidneys confirmed the uptake in the cortex, as observed on the SPECT and PET images, but also showed a very irregular distribution of the cortical radioactivity uptake. The highest uptake was centered in the juxtamedullary (JM) region of the cortex, which was histologically identified as healthy kidney. A striped pattern protruded to the outer regions of the cortex with a reduction of radioactivity uptake density in the outer cortex caused by its divergence. The medulla also showed regional variations in uptake; in general, the central part of the medulla showed the highest uptake. The regions bordering the cortex, however, showed lower uptake and also the striped pattern in the cortical uptake ends abruptly at the corticomedullary boundary. These findings are illustrated in the top left graphs of Figures 1A–1C.

The objective of this study was to design a calculation model for the dose to the kidneys and its subregions for ^{90}Y, ^{111}In, and ^{177}Lu, based on the observed inhomogeneous activity distributions inside the kidneys. Isodose curves for the 2-dimensional (2D) radioactivity distribution have been derived from the kidney autoradiographs. Dose−volume histograms (DVHs) for an extrapolated 3-dimensional (3D) activity distribution inside the stylized kidney model of MIRD19 are compared with homogeneous distributions. Analysis of DVHs of the kidney is considered to be essential in developing accurate dose−effect relationships for renal tolerance (*2,14*). Both the effects of inhomogeneities and therapy fractionation with the LQ model should be incorporated in a radiation nephrotoxicity threshold model for PRRT.

MATERIALS AND METHODS

Autoradiogram data of kidney samples from 3 patients with renal tumors were used. The methods used in gathering the ex vivo autoradiographs were described earlier (*13*). In brief: the male patients were injected with 220 MBq ^{111}In DTPA-octreotide 2–4 d before nephrectomy. Disease-free kidney tissue sections of 10-μm thickness were exposed for 1 d to a phosphor imaging screen (Packard Instruments). The screens were analyzed with a Cyclone phosphor imager (Packard) with a spatial resolution of 500 μm for ^{111}In.

The radioactivity distributions from the autoradiography data files were averaged over 4 × 4 pixel elements for the kidney samples obtained at 96 h (Fig. 1A) and at 72 h (Fig. 1B). The finer structure in the activity distribution of the sample at 48 h (Fig. 1C) made averaging over 3 × 3 pixels necessary. Pixel size was 0.092 mm/pixel. The averaging was performed to reduce the amount of input data and computation time. Furthermore, the resulting sizes of the voxels (0.37 and 0.28 mm, respectively) are more in proportion to the spatial resolution of the imager. Boundary surfaces were fitted to the autoradiographs, both on the outside border of the kidney and also between the cortex and medulla. The averaging and fitting was performed with the Matlab code (The Mathworks, Inc.). The equations for these surfaces were used to define the kidney segments in the Monte Carlo code MCNP5 (*15*) (Oak Ridge National Laboratory, Los Alamos, NM). The segments were made 1-cm thick to generate a 3D structure. The segments were superimposed by a rectangular grid structure corresponding to the averaging voxels ($0.37 \times 0.37 \times 10$ mm^3 for Figs. 1A and 1B and $0.28 \times 0.28 \times 10$ mm^3 for Fig. 1C) for both the source definition and the dose calculation.

A stylized model of the 3D activity distribution was made for the MCNP5 code inside the MIRD19 multiregion kidney phantom (*8*) and is shown in Figure 2. The volumes of cortex, medulla, and pelvis were superimposed with 3-mm-sized voxels. Inside the voxels in the cortex volume cylinders of 1.7-mm diameter were positioned in the center to represent the streaky uptake pattern seen on the autoradiograph. The activity distribution in the 3D model was according to the average distributions on the 3 autoradiographs indicated in Table 1 (*13*). The cortex high radioactivity is assigned to the central cylinders in the voxels and to a 1.8-mm-thick region in the cortex aligning the medulla (JM region). The cortex low radioactivity is assigned to the remaining voxels in the cortex. The activity distribution in the medulla was assumed to be homogeneous, as the autoradiography results do not show the

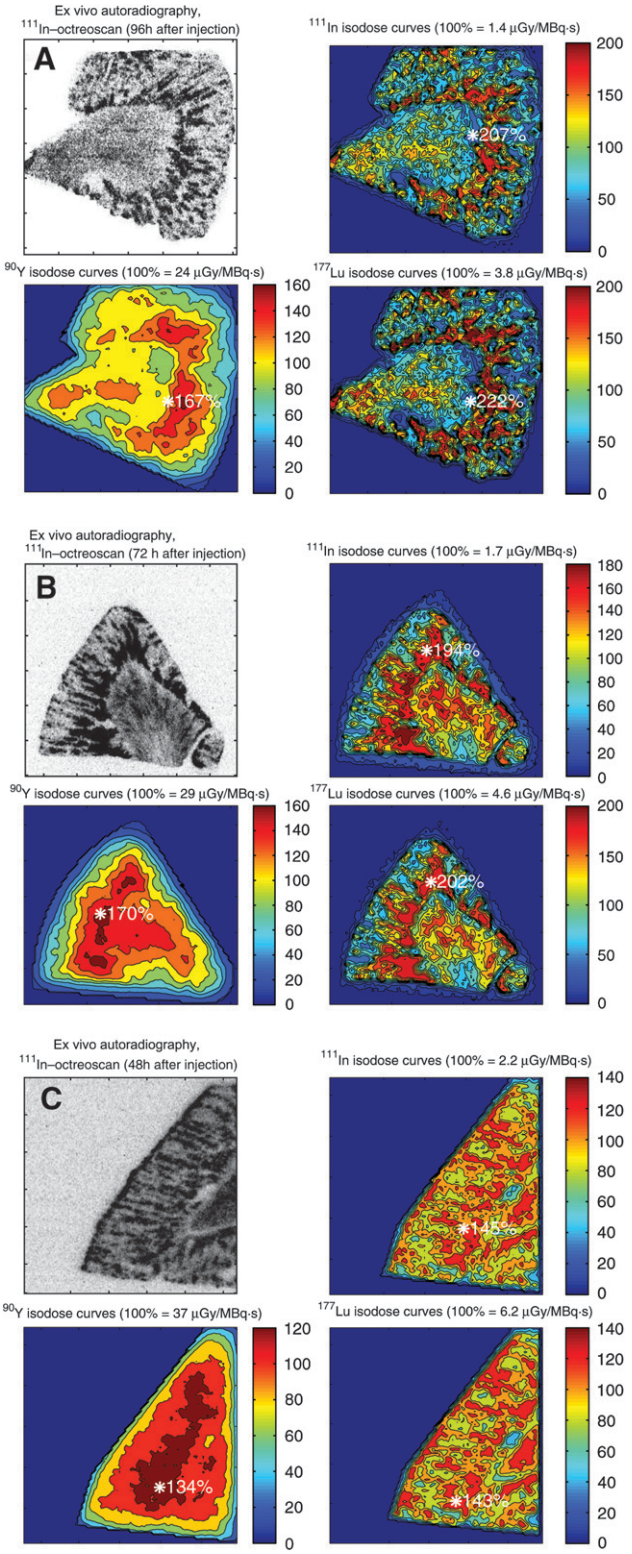

FIGURE 1. Ex vivo autoradiographs of kidney sections from 3 patients (A, B, and C) at different time intervals after administration of ^{111}In-DTPA-octreotide. Dose factors are normalized to average dose to kidney segment, and isodose curves for ^{111}In, ^{90}Y, and ^{177}Lu are 10%, 20%, 40% and, hence, with 20% increment to the maximum. Asterisk indicates position and value of maximum isodoses.

level of heterogeneity found in the cortex. This model is referred to as 3D voxel.

As the reference condition, a homogeneous radioactivity distribution of 70.8% in the cortex and 29.2% in the medullae was considered. Two methods were applied to calculate the kidney dose for this situation. The data from MIRD19 were used for method 1 (named as MIRD19). In the second method the same 3-mm voxel structure was superimposed over the MIRD19 kidney model, without the central cylinder inhomogeneity, however (named as M19 voxel).

The Monte Carlo calculations with MCNP5 were performed to calculate the radiation transport inside the geometries for the high-energy β-emitter ^{90}Y; the γ-ray, low-energy β-ray, and internal conversion electron emitter ^{177}Lu; and the γ-ray and Auger electron emitter ^{111}In. The emission data were obtained from the RADAR Web site (*16*). The typical number of particle histories necessary to constrain statistical fluctuations in the total energy absorbed for each voxel below 5% was 10 million for the electrons and 3 million for the γ-rays. MCNP computing times were approximately 50 h for the β-rays and approximately 100 h for the γ-rays on a 3-GHz personal computer.

A substantial part in the Auger electron spectrum (13% of energy emitted) of ^{111}In is below the lowest energy threshold for MCNP of 1 keV. As no electron tracks are generated below this threshold, MCNP discards the energy emitted by these low-energy Auger electrons. The missing energy was added to the source voxels in the postprocessing phase.

The output data were analyzed with Matlab and Excel (Microsoft Corp.) software to produce isodose curves and DVHs. Summation of the different radiation components of the deposited energy for ^{111}In and ^{177}Lu was also performed in Matlab. The dose per decay to each voxel was calculated by dividing the deposited energy by its voxel mass. The relative biological effectiveness was equal to one for each component (β-rays, γ-rays, or low-energy (Auger) electrons). Both the dose distributions and the average dose to each kidney segment in the MIRD19 model were calculated to enable comparison with the published data from MIRD19.

RESULTS

2D Isodose Curves

The isodose curves for the 3 kidney segments show distinct features of the radiation characteristics of ^{90}Y, ^{111}In, and ^{177}Lu (Fig. 1). With ^{90}Y hardly any features of the uptake pattern are visible, apart from the increased dose to the cortex, whereas for ^{111}In and ^{177}Lu it follows more-or-less the radioactivity uptake pattern. ^{90}Y also shows a larger dose gradient toward the outer surfaces of the cortex in comparison with the other 2 radionuclides, due to loss of the longer-ranged β-particles to the surrounding tissue. The maximum dose for all radionuclides is situated in the JM region.

The absorbed fractions of energy for the 3 autoradiography datasets in the cortex and medulla are compared in Table 2 with the values found for the 3D voxel model and for the homogeneous distribution MIRD19 kidney models (MIRD19 and M19 voxel). The results for autoradiographs A and B were in good agreement with the MIRD19 values for the β-rays and low-energy electrons. The x-rays and γ-rays, however, show lower absorbed energy fractions in the 2D models compared with the MIRD19 3D models.

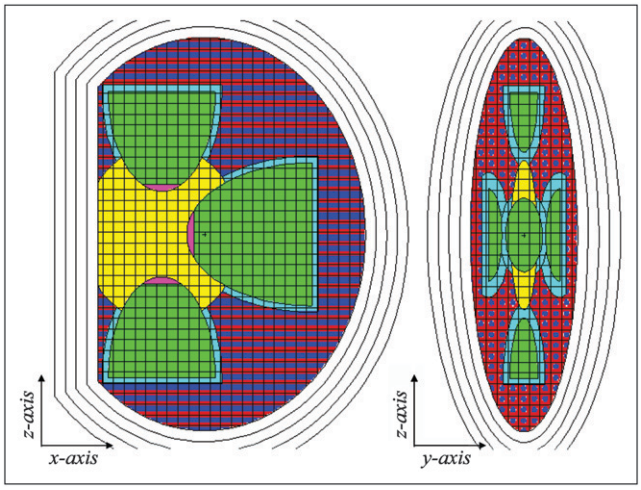

FIGURE 2. Adult-size MIRD19 multiregion kidney model in sagittal view ($x-z$) on left and in coronal view ($y-z$) on right, with overlying 3-mm-voxel grid in medullae (green), pelvis (yellow), and cortex (blue/red pattern). Voxels in cortex were given a 1.7-mm cylindric core representing medullary rays (MR in dark blue); together with a 1.8-mm-thick JM (in light blue) region they form the high-activity-uptake volume. Low-uptake cortex volume (non-MR) is shown in red. Papillae were not voxelized and are colored purple.

The dose factors, or dose per cumulated activity, for the various intraregion source target combinations are given in Table 3. The average doses to the cortex and medullae for the inhomogeneous activity were within 5% from the published MIRD19 values. For ^{177}Lu, however, the reduction by the inhomogeneous activity distribution in the dose to the cortex is substantial: 11%. Because of the large γ-ray component in the dose, the dose reduction in the cortex for ^{111}In was negligible. A reduction in dose to the cortex regions in between the medullary rays (non-MR) was determined as 34% for ^{90}Y, 44% for ^{111}In, and 76% for ^{177}Lu in comparison with the average cortex dose. The contribution to the cortex dose for ^{111}In by the Auger electrons below 1 keV was 7.6% of the total dose.

TABLE 1
Radioactivity Distribution and Volumes of Kidney Regions Inside MIRD19 Kidney Model with High-Uptake (65 %IA) and Low-Uptake (5.8 %IA) Cortex Regions

Region	Radioactivity (%)	Volume (cm^3)
High cortex		
JM	32.4	20.2
MR	32.5	20.4
Low cortex		
Non-MR	5.8	60.0
Medulla	29.2	35.8

%IA = percentage injected activity.
High radioactivity pattern in cortex is subdivided into JM region and medullary ray (MR) region. Low radioactivity pattern is named non-MR. Each region is indicated in Figure 2.

DVHs

DVHs for the 3 radionuclides are shown in Figures 3, 4, and 5 for the homogeneous and inhomogeneous radioactivity distributions. The normalization of the dose was based on the MIRD19 dose to the cortex, which was set to a mean dose of 27 Gy. The DVHs for the homogeneous distribution show an almost block form around the average dose with deviations being caused by the penetrative nature of the radiation; ^{111}In with its γ-rays and ^{90}Y with its high-energy β-particles show a more shallow curve in comparison with the low-energy β-emitter ^{177}Lu. The DVH for the kidney volume resembles that for the cortex volume, apart from the low dose part for ^{177}Lu and, to a lesser extent, for ^{90}Y, where the zero to low dose to the pelvis (4.3% of the kidney volume) manifests itself. In the dose region between 20 and 30 Gy, the dose to the medulla shows up as a shoulder in the reduction of the kidney volume. Although the irradiation differs quite strongly from inhomogeneous irradiation by external x-ray beams, the same methods (*17*) can be used to extract effective volumes from these DVHs. Effective volumes together with other DVH characteristics are summarized in Table 4.

When the radioactivity is assumed to be homogeneously distributed, 5% of the kidney volume would get a dose above 31–32 Gy (D_{05}) for all nuclides. The location of this maximum was outside the cortex, as the cortex D_{05} ranges between 27 and 30 Gy. The relative volumes receiving 70% of the mean dose of (70% x 27 =) 18.9 Gy (V_{70}) are for the homogeneous distribution around 75% of the total renal volume.

With the heterogeneous radioactivity distribution D_{05} rises considerably for ^{111}In and ^{177}Lu to 39 and 46 Gy, respectively. The maximum dose is then found within the cortex. V_{70} drops by 30% with the heterogeneous distribution and for the cortex even by 40%. The effective volume (*17,18*) shows the lowest values for the heterogeneous distribution of ^{177}Lu.

DISCUSSION

In nuclear medicine traditionally doses are based on volume-averaged uptake values over the region of interest (ROI) using the planar imaging conjugate view method. With this method the only possible outcome is a mean dose to the organ by fitting a time–activity curve to the ROI data and using the resulting cumulated activity as input for a dosimetry code, such as OLINDA (*16*). With quantitative PET and in future quantitative SPECT imaging, activity uptake patterns can be measured 3-dimensionally. Ideally, also the dosimetry will have to go to 3 dimensions. In PRRT with, for example, ^{90}Y-DOTA-Tyr^3-octreotide it is of great importance to know the constraints in using average kidney dose as a predictor of end-stage renal disease. Replacing average dose by DVHs may be necessary for short-range β-emitters and electron emitters when the activity is heterogeneously distributed.

TABLE 2
Absorbed Fractions of Energy Emitted by ^{90}Y, ^{111}In, and ^{177}Lu in Cortex and Medulla for 2D Autoradiographies A, B, and C, for 3D models with 70.8% of Activity in Cortex and 29.2% in Medulla

Model	Region	^{90}Y β-ray (%)	^{111}In γ-ray (%)	^{111}In electron (%)	^{111}In x-ray (%)	^{177}Lu β-ray (%)	^{177}Lu γ-ray (%)
A	Cortex	57.5	1.67	66.7	16.9	66.6	1.64
	Medulla	31.8	0.98	32.9	9.9	32.9	0.96
B	Cortex	62.3	1.78	68.7	18.1	68.7	1.74
	Medulla	29.3	0.83	30.4	8.5	31.1	0.81
C	Cortex	76.1	1.99	89.9	20.6	89.6	1.95
	Medulla	8.4	0.23	9.5	2.4	9.5	0.23
MIRD19	Cortex	64.3	4.81	70.3	43.1	70.0	4.81
	Medulla	27.7	1.96	29.2	17.6	29.2	1.96
M19 voxel	Cortex	67.1	4.89	70.8	31.7	70.7	4.86
	Medulla	26.6	2.06	29.1	14.3	29.1	2.12
3D voxel	JM cortex	26.3	1.21	32.1	8.6	31.9	1.20
	MR cortex	12.8	0.93	29.4	6.1	27.4	0.92
	Non-MR	26.1	2.55	9.1	16.3	11.1	2.56
	Total cortex	65.2	4.69	70.6	31.0	70.5	4.86
	Medulla	30.8	2.25	29.6	15.9	29.3	2.31

MIRD19 data were derived from MIRD19 (*8*) for homogeneous activity distributions in cortex and medullae. M19 voxel model is also for homogeneous activity distribution inside a 3-mm voxelized MCNP model of MIRD19 kidney. Heterogeneous activity distribution, given in Table 1, is used in the 3D voxel model, shown in Figure 2. In the 3D voxel model, 3 regions are defined in cortex: JM, medullary rays (MR), and non-MR, with the sum in total cortex.

There is little knowledge on the effect of heterogeneous dose distributions in the kidneys. In rats the effects of regional distribution of the renal radioactivity uptake has been studied as a function of the size of the antibody to which the radionuclide is linked (*19*). More efficient filtering of smaller antibodies by the glomeruli relatively increases the cortical uptake. Peptide reabsorption occurs in the proximal tubules. Isodose curves were calculated and showed that the combination of short-ranged radiation and small-size antibodies (or peptides) made separate dose calculations for the rat cortex and medulla necessary.

The heterogeneous uptake pattern of ^{111}In-DTPA-octreotide in the human kidney has a large influence on the dose distribution inside the kidney, especially for short-range β-emitters and electron emitters. The calculated isodose curves for ^{111}In and ^{177}Lu show steep gradients between the regions with high and low radionuclide uptake. DVHs are a better instrument for evaluating the differences between the 3 radionuclides considered in this study. Especially ^{177}Lu seems promising in tolerating higher kidney doses in comparison with ^{111}In and ^{90}Y. With an average dose of 27 Gy to the cortex, 60% of the cortex volume (D_{40}) receives a dose below 7.1 Gy with ^{177}Lu.

TABLE 3
Renal Element Dose Conversion Factors (DF) for the 3D Models Defined in Table 2

	DF (mGy/MBq·s)						
Model	Kidney	Cortex	JM cortex	MR cortex	Non-MR	Medulla	Pelvis
				^{90}Y			
MIRD19	4.86E−04	4.78E−04				5.78E−04	1.18E−04
M19 voxel	4.73E−04	4.80E−04				5.35E−04	5.67E−05
3D voxel	4.69E−04	4.67E−04	9.36E−04	4.51E−04	3.14E−04	5.60E−04	4.51E−05
				^{111}In			
MIRD19	3.83E−05	3.79E−05				4.39E−05	1.67E−05
M19 voxel	3.83E−05	3.79E−05				4.49E−05	1.74E−05
3D voxel	3.88E−05	3.77E−05	6.66E−05	6.40E−05	2.12E−05	4.71E−05	1.91E−05
				^{177}Lu			
MIRD19	8.31E−05	8.36E−05				9.77E−05	2.92E−06
M19 voxel	8.05E−05	8.13E−05				9.40E−05	1.14E−06
3D voxel	7.39E−05	7.44E−05	1.67E−04	1.43E−04	1.99E−05	8.71E−05	1.32E−06

See definitions in legend to Table 2.

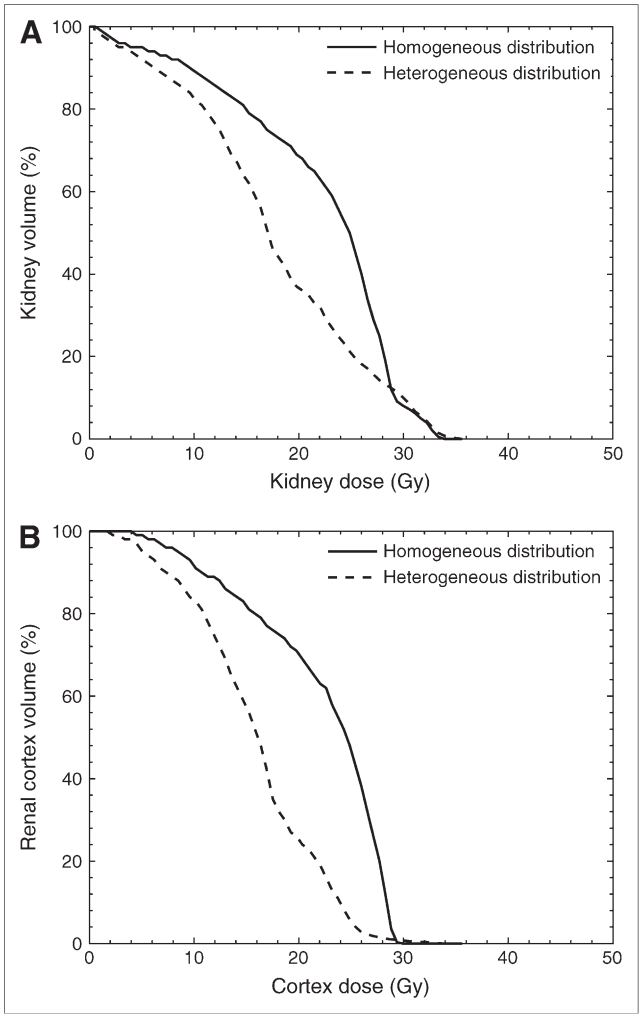

FIGURE 3. DVHs for kidney (A) and cortex (B) for ^{90}Y source activity: 71% in cortex and 29% in medullae in either a homogenous distribution or a distribution following the mean autoradiograph results. Average dose to cortex was taken as 27 Gy, calculated according to MIRD19 (*8*).

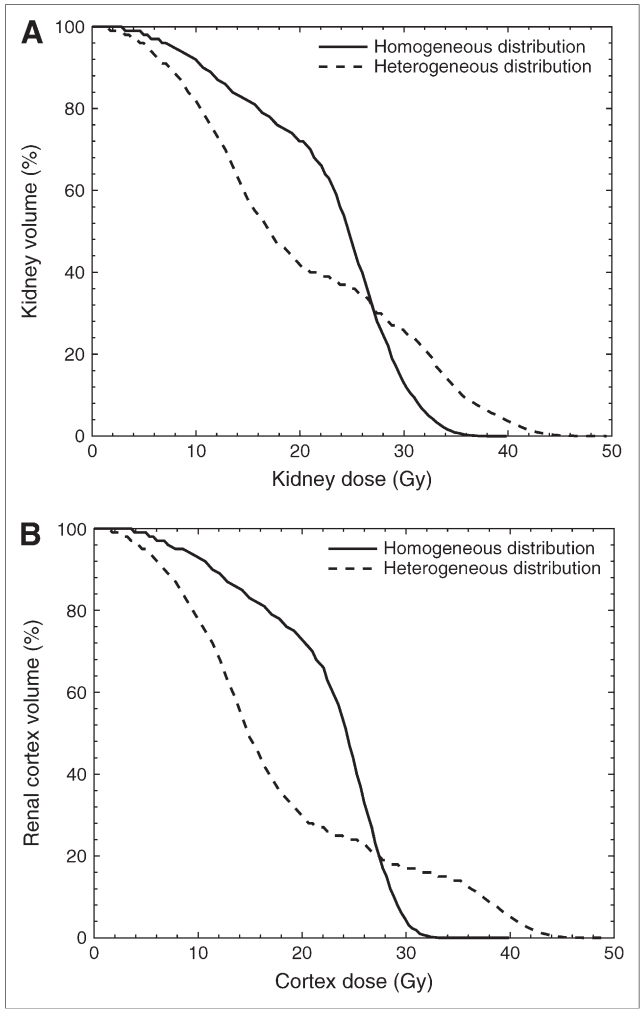

FIGURE 4. DVHs for kidney (A) and cortex (B) for ^{111}In source activity: 71% in the cortex and 29% in medullae in either a homogenous distribution or a distribution following the mean autoradiograph results. Average dose to cortex was taken as 27 Gy, calculated according to MIRD19 (*8*).

^{111}In gives a D_{40} below 17 Gy, and ^{90}Y shows a D_{40} of 17.5 Gy. The maximum dose to the cortex is, however, the highest for ^{177}Lu: 5% of the cortex volume (D_{05}) gets a dose above 47 Gy, whereas ^{111}In gives a D_{05} of 40 Gy and ^{90}Y gives a D_{05} of 25 Gy.

Differences between the dose conversion factors derived from MIRD19 and the values for homogeneous voxelized distribution are evident for ^{90}Y and ^{177}Lu. This could be due to the use of different Monte Carlo codes; for MIRD19 the EGS code was used, whereas in this work MCNP was used. Also the voxel structure may cause boundary problems, such as partial-volume effects in voxels crossing the kidney−region boundaries.

By focusing on the dose to the cortex we assume that this region is responsible for the radiation-induced end-stage renal disease observed after radionuclide therapy in some patients. The experience in external beam radiotherapy (XRT) kidney dosimetry is quite contrary compared with PRRT: The dose to the outer regions of the cortex is lower than that to the regions bordering the medulla. Also the heterogeneity in the radioactivity uptake in the kidneys for PRRT could very well show us the functional subunits (FSUs) of the kidney: the nephrons. Unfortunately, it has not been possible to get good histology of the tissue responsible for the heterogeneous renal radioactivity uptake pattern of ^{111}In-DTPA-octreotide. It is then questionable whether the radiation dose–response of the kidneys still can be considered to follow the behavior typical for parallel structures; in external beam therapy this was concluded from the fact that the critical fraction of FSUs needed to maintain kidney function was determined to be 0.77 (*20*). Adjacent unirradiated FSUs will take over the function of the irradiated FSUs, and cell migration from the unirradiated part to the irradiated elements may restore the functional status of the kidney.

The structure of the radiation damage with PRRT is, however, very different; it is expected to be maximal in the

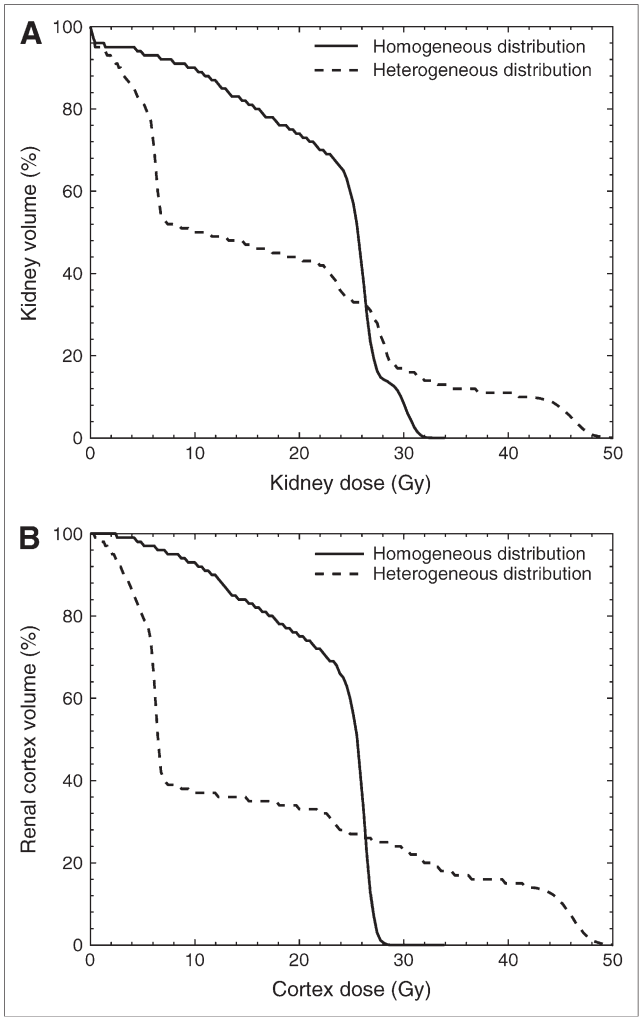

FIGURE 5. DVHs for kidney (A) and cortex (B) for ^{177}Lu source activity: 71% in cortex and 29% in medullae in either a homogenous distribution or a distribution following the mean autoradiograph results. Average dose to cortex was taken as 27 Gy, calculated according to MIRD19 (*8*).

JM region with all tubuli leading into the medulla. When all tubuli in this region get doses well above the threshold for damage, no neighboring elements will remain to take over their function. Whether cell migration from up- or downstream unirradiated parts of the affected tubuli is fast enough to repair its function seems unlikely. However, the observed clinical experience is that high-dose ^{111}In-DTPA-octreotide and ^{90}Y-DOTA-Tyr^3-octreotide therapy, with average kidney doses of 27 Gy, leading to JM doses of 39 and 32 Gy, respectively, for the heterogeneous distribution was given without subsequent major renal problems (*1*). More specifically, the tubular function showed no clinically relevant deterioration, either shortly after PRRT or during long follow-up. Therapy with ^{177}Lu-DOTA-Tyr^3-octreotate at an average kidney dose of 23 Gy, which still leads to a JM dose of 40 Gy, is reported to be even less toxic to the kidneys. The distribution and the size of the glomeruli in the cortex are not homogeneous (*21,22*), but it is unclear whether this also reflects their contribution to the total kidney function. High doses to the JM regions in the cortex could very well devastate the glomeruli in that region, so the renal function must be maintained only by the glomeruli in the outer cortex. Still, both in the dose–response of the kidney (*6*) as in the clinical pattern of radiation-induced renal disease by PRRT, no overt unexplained differences were observed from the situation after kidney radiation exposure by XRT.

A commonly applied method in XRT for reducing the DVH data to a single dose parameter is the effective volume method (*17,18*). Each voxel for a parallel structured organ obeys the same dose–volume relationship as the whole organ. The tolerance dose TD(v) after uniform radiation to a partial volume v depends on the tolerance dose for uniform irradiation of the whole organ (v = 1) by the Lyman equation: $TD(v) = TD(1) \cdot v^{-n}$ .The volume dependence parameter $n = 0.7$ (*23*) was obtained by fitting to the kidney tolerance data of Emami et al. (*24*). Each step in the kidney DVH of volume ΔV_i with dose D_i is then transformed to an effective volume in the adjacent dose bin with higher dose, which is iterated until each volume section of the DVH is transformed to the effective volume with a maximum dose D_m by:

$$V_{eff} = \sum_{i=1}^{m-1} \left(D_i \Big/ D_m \right)^{1/n} \Delta V_i.$$

The effective volumes for ^{90}Y, ^{111}In, and ^{177}Lu are given in Table 4. Homogeneous radioactivity distribution in the cortex creates a dose distribution as if just 56% (^{111}In) to 72% (^{177}Lu) of the cortex volume is homogeneously irradiated with the maximum dose of 30 Gy and 27 Gy, respectively. When the activity is distributed according to the autoradiography data the effective volume drops especially for ^{177}Lu to 24% with a higher maximum at 47 Gy. In the case of ^{90}Y the effective volume shows a lower decrease when introducing heterogeneity, but also the maximum drops from 29 to 25 Gy, as the MIRD19-based dosimetry overestimates the dose to the cortex for inhomogeneous ^{90}Y activity distribution.

In PRRT there is hardly any possibility of actively shaping its DVH to a safer profile, unlike in XRT. The only possibility would be to change from ^{90}Y to ^{177}Lu, when the activity is distributed heterogeneously. Again, it must be stressed that partial irradiation in XRT fields is very different from the dose heterogeneity observed with PRRT. In XRT either a single kidney or the upper poles of both kidneys are irradiated. It is, however, logical to expect that the threshold for late kidney radiation damage after therapy with ^{177}Lu-DOTA-Tyr^3-octreotate will show an even higher shift from the external beam threshold than that observed with ^{90}Y-DOTA-Tyr^3-octreotide, both due to the heterogeneous dose distribution as well as due to the longer half-life. Taking the Lyman equation literally, this shift for the effective volume of 24% for ^{177}Lu will be a factor of ($v^{-n} = 0.24^{-0.7} =$) 2.7.

TABLE 4
Summary DVH Data for Homogeneous and Heterogeneous Activity Distribution in Kidney Based on a 27-Gy Dose to Cortex Following MIRD19 (*8*)

Parameter	Homogeneous distribution			Heterogeneous distribution		
	^{90}Y (%)	^{111}In (%)	^{177}Lu (%)	^{90}Y (%)	^{111}In (%)	^{177}Lu (%)
Kidney						
D_{mean}	27 Gy	27 Gy	26 Gy	27 Gy	28 Gy	24 Gy
D_{05}	32 Gy	32 Gy	31 Gy	32 Gy	39 Gy	46 Gy
V_{70}	72	75	76	42	46	44
V_{95}	45	42	52	20	35	33
V_{eff}	57	50	60	40	31	26
Cortex						
D_{mean}	27 Gy	27 Gy	26 Gy	26 Gy	27 Gy	24 Gy
D_{05}	29 Gy	30 Gy	27 Gy	25 Gy	40 Gy	47 Gy
V_{70}	74	76	77	30	34	34
V_{95}	43	37	51	4	23	27
V_{eff}	68	56	72	37	27	24

D_{mean} = mean dose; D_{05} = dose encompassing 5% of volume; V_{70} = volume receiving 70% or more (>18.9 Gy) of prescribed dose; V_{95} = volume receiving 95% (>25.7 Gy) of dose; V_{eff} = effective volume (*18*).

In reality this shift will be lower, as the observed heterogeneity is undoubtedly a transient situation, but even with the homogeneous activity distribution V_{eff} = 72% leads to a shift in tolerance dose with a factor of 1.26. This would indicate a tolerance dose for ^{177}Lu of 29 Gy instead of 23 Gy.

CONCLUSION

Heterogeneous radioactivity distribution in the kidneys has only consequences to the dose distribution for low-energy β-emitters and electron emitters such as ^{111}In and ^{177}Lu. Large volumes of the cortex get smaller doses than average with ^{111}In and ^{177}Lu. The higher doses to the kidney regions with high radioactivity uptake do not create a higher incidence of renal damage in clinical practice compared with therapy with ^{90}Y. The use of DVHs instead of average doses is strongly advocated for all radionuclides considered, irrespective of any heterogeneity in activity distribution over the kidney. In the case of the short- and medium-range electron emitters, such as ^{111}In and ^{177}Lu, DVHs give a better indication of relative volumes that will exceed tolerance doses. PRRT based on ^{90}Y, emitting longer-ranged β-rays, will create more dose averaging inside the kidney regions. The consequences of heterogeneous dose distribution in the kidney for radiation damage to its functional subunits are not clear. However, if it follows the Lyman relationship, an additional sparing of the kidney of minimally a factor 1.25 can be expected. It is, however, rarely possible to obtain activity distribution data on the tissue level.

REFERENCES

1. Valkema R, Pauwels SA, Kvols LK, et al. Long-term follow-up of renal function after peptide receptor radiation therapy with ^{90}Y-DOTA,Tyr^3-octreotide and ^{177}Lu-DOTA^0, Tyr^3-octreotate. *J Nucl Med.* 2005;46(suppl):83S–91S.
2. Cassady JR. Clinical radiation nephropathy. *Int J Radiat Oncol Biol Phys.* 1995; 31:1249–1256.
3. Walrand S, Jamar F, Mathieu I, et al. Quantification in PET using isotopes emitting prompt single gammas: application to ^{86}Y. *Eur J Nucl Med Mol Imaging.* 2003;30:354–361.
4. Moll S, Nickeleit V, Mueller-Brand J, Brunner FP, Maecke HR, Mihatsch MJ. A new cause of renal thrombotic microangiopathy: yttrium 90-DOTATOC internal radiotherapy. *Am J Kidney Dis.* 2001;37:847–851.
5. Cybulla M, Weiner SM, Otte A. End-stage renal disease after treatment with ^{90}Y-DOTATOC. *Eur J Nucl Med.* 2001;28:1552–1554.
6. Barone R, Borson-Chazot F, Valkema R, et al. Patient-specific dosimetry in predicting renal toxicity with ^{90}Y-DOTATOC: relevance of kidney volume and dose rate in finding a dose-effect relationship. *J Nucl Med.* 2005;46(suppl): 99S–106S.
7. Konijnenberg MW. Is the renal dosimetry for [^{90}Y-DOTA^0,Tyr^3]octreotide accurate enough to predict thresholds for individual patients? *Cancer Biother Radiopharm.* 2003;18:619–625.
8. Bouchet LG, Bolch WE, Blanco HP, et al. MIRD Pamphlet No 19: absorbed fractions and radionuclide S values for six age-dependent multiregion models of the kidney. *J Nucl Med.* 2003;44:1113–1147.
9. Dale R. Use of the linear-quadratic radiobiological model for quantifying kidney response in targeted radiotherapy. *Cancer Biother Radiopharm.* 2004;19: 363–370.
10. Kwekkeboom DJ, Teunissen JJ, Bakker WH et al. Radiolabeled somatostatin analog [^{177}Lu-DOTA^0,Tyr^3]octreotate in patients with endocrine gastroenteropancreatic tumors. *J Clin Oncol.* 2005;23:2754–2762.
11. Valkema R, De Jong M, Bakker WH, et al. Phase I study of peptide receptor radionuclide therapy with [In-DTPA]octreotide: the Rotterdam experience. *Semin Nucl Med.* 2002;32:110–122.
12. Helisch A, Forster GJ, Reber H, et al. Pre-therapeutic dosimetry and biodistribution of ^{86}Y-DOTA-Phe^1-Tyr^3-octreotide versus ^{111}In-pentetreotide in patients with advanced neuroendocrine tumours. *Eur J Nucl Med Mol Imaging.* 2004;31:1386–1392.
13. De Jong M, Valkema R, Van Gameren A, et al. Inhomogeneous localization of radioactivity in the human kidney after injection of [^{111}In-DTPA]octreotide. *J Nucl Med.* 2004;45:1168–1171.
14. Adelstein SJ, Green AJ, Howell RW, et al. ICRU report 67: absorbed-dose specification in nuclear medicine. *J ICRU.* 2002;2:64–65.
15. Las Alamos National Laboratory Report: LA-UR-03-1987; MCNP—A general Monte Carlo N-particle transport code [report on CD-ROM]. Version 5. Booth TE, Brown FB, Bull JS, et al., eds. Las Alamos, NM: Las Alamos National Laboratory; 2003.
16. Stabin MG, Sparks RB, Crowe E. OLINDA/EXM: the second-generation personal computer software for internal dose assessment in nuclear medicine. *J Nucl Med.* 2005;46:1023–1027.

17. Kutcher GJ, Burman C. Calculation of complication probability factors for non-uniform normal tissue irradiation: the effective volume method. *Int J Radiat Oncol Biol Phys.* 1989;16:1623–1630.
18. Kutcher GJ, Burman C, Brewster L, Goitein M, Mohan R. Histogram reduction method for calculating complication probabilities for three-dimensional treatment planning evaluations. *Int J Radiat Oncol Biol Phys.* 1991;21:137–146.
19. Flynn AA, Pedley RB, Green AJ, et al. The nonuniformity of antibody distribution in the kidney and its influence on dosimetry. *Radiat Res.* 2003;159:182–189.
20. Olsen DR, Kambestad BK, Kristoffersen DT. Calculation of radiation induced complication probabilities for brain, liver and kidney, and the use of a reliability model to estimate critical volume fractions. *Br J Radiol.* 1994;67:1218–1225.
21. Skov K, Nyengaard JR, Patwardan A, Mulrany MJ. Large juxtamedullary glomeruli and afferent arterioles in healthy primates. *Kidney Int.* 1999;55:1462–1469.
22. Newbold KM, Sandison A, Howie AJ. Comparison of size of juxtamedullary and outer cortical glomeruli in normal adult kidney. *Virchows Arch A Pathol Anat Histopathol.* 1992;420:127–129.
23. Burman C, Kutcher GJ, Emami B, Goitein M. Fitting of normal tissue tolerance data to an analytic function. *Int J Radiat Oncol Biol Phys.* 1991;21:123–135.
24. Emami B, Lyman J, Brown A, et al. Tolerance of normal tissue to therapeutic irradiation. *Int J Radiat Oncol Biol Phys.* 1991;21:109–122.